

# Enhancing Semantic Segmentation with Adaptive Focal Loss: A Novel Approach

Md Rakibul Islam<sup>1</sup>, Riad Hassan<sup>2,3</sup>, Abdullah Nazib<sup>4</sup>, Kien Nguyen<sup>4</sup>, Clinton Fookes<sup>4</sup>, and Md Zahidul Islam<sup>1</sup>

- <sup>1</sup> Dept. of Information & Communication Technology, Islamic University, Bangladesh  
 rakibuliuct@gmail.com<sup>[0009-0007-0881-7014]</sup>,  
 zahidimage@gmail.com<sup>[0000-0002-8072-7896]</sup>,  
<sup>2</sup> ICT, Bangladesh University of Engineering and Technology.  
<sup>3</sup> Department of CSE, Green University of Bangladesh.  
 riad@cse.green.edu.bd<sup>[0000-0003-1048-0346]</sup>  
<sup>4</sup> School of Electrical Engineering and Robotics, QUT, Brisbane, Australia.  
 nazib@qut.edu.au<sup>[0000-0003-1048-0346]</sup>, c.fookes@qut.edu.au<sup>[0000-0002-8515-6324]</sup>,  
 k.nguyenthanh@qut.edu.au<sup>[0000-0001-8994-5585]</sup>

**Abstract.** Deep learning has achieved outstanding accuracy in medical image segmentation, particularly for objects like organs or tumors with smooth boundaries or large sizes. Whereas, it encounters significant difficulties with objects that have zigzag boundaries or are small in size, leading to a notable decrease in segmentation effectiveness. In this context, using a loss function that incorporates smoothness and volume information into a model's predictions offers a promising solution to these shortcomings. In this work, we introduce an Adaptive Focal Loss (A-FL) function designed to mitigate class imbalance by down-weighting the loss for easy examples that results in up-weighting the loss for hard examples and giving greater emphasis to challenging examples, such as small and irregularly shaped objects. The proposed A-FL involves dynamically adjusting a focusing parameter based on an object's surface smoothness, size information, and adjusting the class balancing parameter based on the ratio of targeted area to total area in an image. We evaluated the performance of the A-FL using ResNet50-encoded U-Net architecture on the Pical 2022 and BraTS 2018 datasets. On the Pical 2022 dataset, the A-FL achieved an Intersection over Union (IoU) of 0.696 and a Dice Similarity Coefficient (DSC) of 0.769, outperforming the regular Focal Loss (FL) by 5.5% and 5.4% respectively. It also surpassed the best baseline Dice-Focal by 2.0% and 1.2%. On the BraTS 2018 dataset, A-FL achieved an IoU of 0.883 and a DSC of 0.931. The comparative studies show that the proposed A-FL function surpasses conventional methods, including Dice Loss, Focal Loss, and their hybrid variants, in IoU, DSC, Sensitivity, and Specificity metrics. This work highlights A-FL's potential to improve deep learning models for segmenting clinically significant regions in medical images, leading to more precise and reliable diagnostic tools.

**Keywords:** Adaptive Focal Loss · Semantic Segmentation · Deep Learning · ResNet50-encoded U-Net · Class Imbalance · Tumor Segmentation.

## 1 Introduction

Precise segmentation of affected regions is essential for optimal outcomes in robotic surgery, computer-aided diagnostics, and targeted radiation therapy [24]. The targeted region declination is tedious and time consuming. Recent advancement in deep neural network increases the performance of segmentation and it is relatively high when the shape of the targeted segmentation region is large and comparatively smooth. But the segmentation is challenging when the objects are with small size or zigzag boundary. In recent time, many segmentation networks have been proposed to segment the challenging objects more accurately [1, 12, 13, 17, 18, 26]. Although the features are extracted with the segmentation networks from different view, the performance enhancement is minimal.

Such challenging objects are common for segmentation in medical imaging. Organs, tumors' shapes are not only uneven but also poses variability person to person. Segmentation networks commonly rely on loss functions such as Dice [23], Cross-Entropy [19], and Focal [7], which focus mainly on object overlap and the entropy between predicted and ground truth masks. However, these loss functions often fail to consider critical factors like surface boundary characteristics and object volume, which are crucial for accurate segmentation of small or irregularly shaped objects.

To solve these issues, we introduce a novel Adaptive Focal Loss (A-FL) that considers tumor volume information, surface smoothness information, and dynamically adjusts class balancing parameter. When the objects are ordinary with large size and smooth surface, the A-FL poses lower loss. In contrast, during the challenging object segmentation, the A-FL offer higher loss and force the network to optimize the loss properly. This dynamic adaptive nature of A-FL successfully feedback the loss appropriately to the network which leads the higher segmentation accuracy.

## 2 Related Work

Binary Cross Entropy (BCE) loss [19] and its variations [5, 19, 25], are frequently utilized for model training within the domain of semantic segmentation [6, 8]. The model's performance may be hampered by the simple pixels' gradients being overwhelmed by the hard pixels' due to BCE's equal treatment of all pixels. By correcting the imbalance between positive and negative samples [10, 15], or the disparity between easy and hard samples [5, 7], previous initiatives [14] have attempted to remedy this.

Weighted Binary Cross Entropy (WBCE) [3] introduces a weighting factor for positive samples in order to rectify the imbalance between positive and negative data. In a similar manner, positive and negative samples are given weights via Balanced Cross Entropy (BCE) [25]. These techniques are beneficial when applied to skewed data distributions [4], but their impact on model performance when applied to balanced datasets may be less pronounced. An unique solution to this problem was offered by Leng et al. [5], who proposed Poly Loss (PL), a linear mix of polynomial functions.

Focal Loss (FL) [7] provides a difficulty modifier to address the discrepancy between hard/easy samples. This helps the model concentrate more on hard cases by lessening the influence of easy examples. The Normalized Focal Loss (NFL), which incorporates an extra correction factor inversely related to the modulating component in FL, was proposed by Sofiuk et al. [22]. Other research [10], [15] have also attempted to address this issue; nevertheless, difficulties such as gradient swamping impede the proper classification of equivocal pixels.

In this research by utilizing A-FL in where we introduce a focusing parameter  $\gamma_{adaptive}$  that is dynamically adjusted according to the volume and smoothness information of the segmented objects. This approach aims to overcome the restrictions of static parameter choices encountered in conventional focal loss functions so as to improve the segmentation of irregularly shaped and small sized tumors.

### 3 Methodology

The overall working pipeline of this research implementation is illustrated in Fig.1. It consists of three main components: (a) dataset pre-processing, (b) ResNet50-encoded U-Net architecture, and (c) proposed A-FL function. Details on data pre-processing are provided in Section 4. In this section, we provide a summary of A-FL, detail the implementation of our innovative adaptive focal loss that dynamically integrates tumor volume and surface smoothness information, and describe the segmentation network architecture.

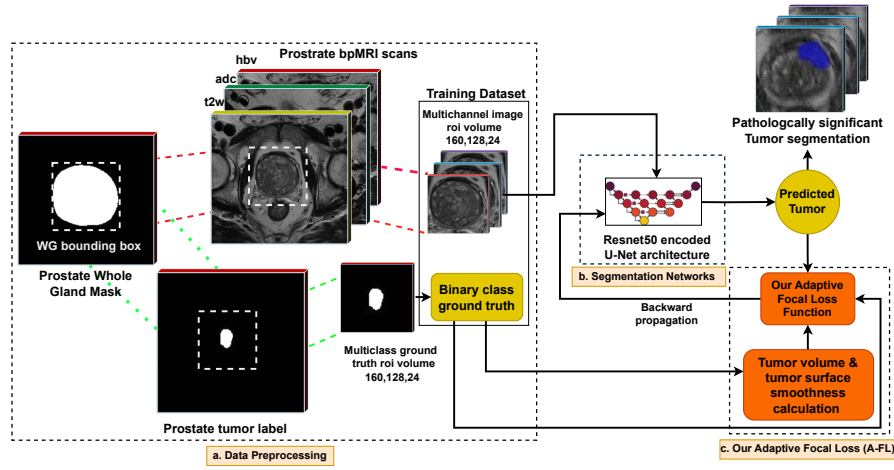


**Fig. 1.** Overall working pipeline comprises of three main parts: a. Data pre-processing; b. Segmentation Network; c. proposed Adaptive Loss Function (A schematic overview of the training process with our Adaptive Loss function (A-FL)).

### 3.1 Overview

The core concept of Adaptive Focal Loss (A-FL) is to dynamically calculate and then incorporate the tumor volume and surface smoothness information into regular Focal loss function through a focusing parameter for each patient during the training process. A-FL uses dynamically calculated non-cancerous pixel to total pixels ratio as class balancing parameter, which helps to address the class imbalance between the numerous non-cancerous pixels and the comparatively few cancerous pixels. As shown in Fig.1 step c, we introduce two straightforward but highly effective modifications to the regular focal loss function during the training process:

1. During training, we assess tumor surface smoothness by computing the gradient along the x, y, and z axes, and we also evaluate tumor volume by calculating the ratio of cancerous pixels to the total pixels in the corresponding label mask. We use this smoothness and volume information as focusing parameter.
2. We calculate the ratio of non-cancerous pixels to the total pixel count and utilize this ratio as a class balancing parameter.

To compute both focusing parameter and class balancing parameter during the training process we have introduced a novel specifically designed mathematical model. This approach is optimized for computational efficiency and integrates seamlessly into the training pipeline. By calculating these parameters dynamically during training, the proposed loss function ensures that the segmentation model can better adapt to variations in tumor sizes and surface characteristics that results in greater accuracy and robustness of the segmentation outcomes.

### 3.2 Tumor volume & surface smoothness aware Adaptive Focal Loss (A-FL)

We used the regular focal loss function [7] as our baseline to focus on easy/hard examples by reshaping the Balanced Cross Entropy loss with a modulating factor that is based on manually tune-able focusing parameter. Their research showed that a fixed focusing parameter of 2 and class balancing parameter of 0.25 yielded the best results. This approach fails to address the varying difficulty levels within the dataset, particularly struggling with small and irregularly shaped tumors. As a result, the model often fails to achieve optimal segmentation accuracy for these challenging examples.

We address these limitations by dynamically adjusting a focusing parameter based on tumor volume and surface smoothness information, and a class balancing parameter based on the non-cancerous to total pixel ratio. This adaptive focal loss effectively handles class imbalance, able to give more focus on hard examples like small or irregularly shaped tumors. By ensuring higher training loss for challenging examples and lower for easy ones, our approach allows the model to update its weights more effectively, improving dice accuracy for small and more zigzag shaped tumors.

In this work, we propose a novel enhancement to the standard Focal loss by dynamically adjusting the focusing parameter during training for semantic segmentation. We term this parameter as Adaptive Focusing Parameter because it is adjusted based on the volume and surface smoothness information of the tumor. The following steps outline the detailed implementation of proposed adaptive focal loss (A-FL):

1. **Calculating Tumor Volume Based Adaptive Parameters:** To address class imbalance and give more focus to small tumor cases, we dynamically calculate the class balancing adaptive parameter and tumor volume information adaptive parameters using the cancerous and non-cancerous pixels ratios to the total pixels for each patient's tumor during training. The equation in 1 and 2 are the mathematical formula of Class Balancing Adaptive Parameter ( $\alpha_{va}$ ) and volume information adaptive parameter.

$$\alpha_{va} = \frac{P_{bg}}{P_{fg} + P_{bg}} \quad (1)$$

$$\gamma_{va} = \frac{P_{fg}}{P_{fg} + P_{bg}} \quad (2)$$

where  $P_{fg}$  represents the count of foreground pixels (non-zero elements) and  $P_{bg}$  represents the count of background pixels (zero elements).

2. **Calculating Mean Surface Smoothness Adaptive Parameter:** To compute the mean smoothness of a patient's mask, we perform the following steps.

*I. Gradients along the x, y, and z Axes:* Let  $I$  be the image tensor. The gradients along the x, y, and z axes are denoted as  $\nabla_x I$ ,  $\nabla_y I$ , and  $\nabla_z I$  respectively, and the formula can be expressed as in Equation 3.

$$\nabla_x I = \frac{\partial I}{\partial x}, \quad \nabla_y I = \frac{\partial I}{\partial y}, \quad \nabla_z I = \frac{\partial I}{\partial z} \quad (3)$$

*II. Gradient Magnitude:* Using the Euclidean norm of the gradients [21] presented in Equation 4, we calculate the magnitude of the gradient at each point along tumor boundary.

$$\|\nabla I\| = \sqrt{(\nabla_x I)^2 + (\nabla_y I)^2 + (\nabla_z I)^2} \quad (4)$$

*III. Mean Smoothness:* The mean surface smoothness adaptive parameter ( $\gamma_{mSa}$ ) is calculated as the average of the gradient magnitudes over the entire image tensor. Let  $N$  be the total number of elements in the image tensor and the formula is as follows:

$$\gamma_{mSa} = \frac{1}{N} \sum_{i=1}^N \|\nabla I_i\| \quad (5)$$

3. **Calculating the Adaptive Focusing Parameter:** The adaptive parameter  $\gamma_{adaptive}$  is then calculated as the sum of the volume adaptive parameter ( $\gamma_{va}$ ) and the mean smoothness adaptive parameter ( $\gamma_{mSa}$ ) as follows:

$$\gamma_{adaptive} = \gamma_{va} + \gamma_{mSa} \quad (6)$$

4. **Defining the Adaptive Focal Loss (A-FL):** Our proposed A-FL denoted as  $A - FL(P_t)$  expands on conventional Focal loss by utilizing dynamically adaptive parameter  $\gamma_{adaptive}$ . The Equation 7 shows the mathematical formula of A-FL.

$$A-FL(P_t) = (1 - P_t)^{\gamma_{adaptive}} \cdot \log(P_t) \quad (7)$$

We note two key properties of our adaptive focal loss (A-FL):

1. When an example is misclassified and  $p_t$  is low, the modulating factor stays near 1, keeping the loss unchanged. On the other hand, as  $p_t$  nears 1, the factor reduces to 0, thus down-weighting the loss for accurately classified examples.
2. The value of the modulating parameter  $(1 - P_t)^{\gamma_{adaptive}}$  changes in response to variations in  $p_t$  for all patients. We have investigated whether the value of  $p_t$  varies based on tumor volume and tumor surface smoothness in each patient. Thus, we incorporate these two factors (volume and smoothness) into our adaptive focusing parameter  $\gamma_{adaptive}$ .

In practice, we have incorporated the class balancing adaptive parameter  $\alpha_{va}$  as defined in Equation 1, into our proposed loss function. This inclusion results in slightly better accuracy compared to the compared to the non- $\alpha_{va}$ -included form. The final A-FL formula is presented in Equation 8.

$$A-FL(P_t) = \alpha_{va} \cdot (1 - P_t)^{\gamma_{adaptive}} \cdot \log(P_t) \quad (8)$$

### 3.3 Our ResNet50 Encoded U-Net Architecture

For all our experiments, we utilize ResNet50 [2] as the encoder in the U-Net architecture. This backbone is extensively employed in semantic segmentation [11], making it an ideal baseline for comparison and future studies. Integrating ResNet50 into U-Net encoder (displayed in Fig. 2) significantly boosts the network’s feature extraction capabilities. The residual blocks in ResNet50 effectively mitigate the vanishing gradient issue, enabling the network to learn more robust and abstract features.

## 4 Experiment Setup

### 4.1 Dataset

All our experiments use two publicly available MRI datasets: 1) the Picai 2022 dataset [20] and 2) the BraTS 2018 dataset [9]. Both datasets are designed to

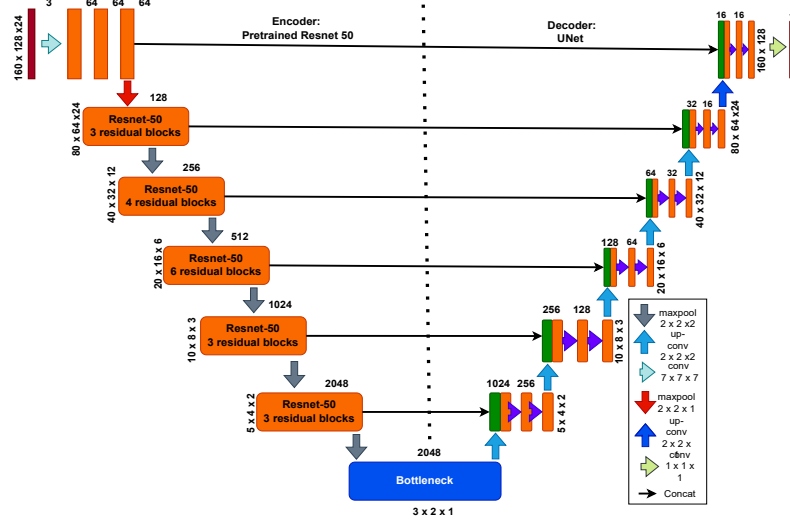


**Fig. 2.** The U-Net network architecture uses pre-trained Resnet50 [2] as backbone. The residual blocks in ResNet50 enable the network to learn more complex features and deeper representations, which are crucial for accurate segmentation.

improve cancer diagnosis using deep learning (DL) tools.

**Picai 2022 dataset:** This dataset includes 1,500 Bi-parametric MRI (bpMRI) cases with three modalities: Apparent Diffusion Coefficient (ADC), High b-value (HBV), and T2-weighted (T2w). It comprises 1,075 benign or indolent prostate cancer (PCa) cases, 205 unlabeled malignant cases, and 220 manually labeled malignant cases. For segmentation model training, 220 patients are utilized, divided into a training set of 180 patients (80%) and a validation set of 40 patients (20%).

**BraTS 2018 dataset:** This dataset includes multi-modal MRI scans from 650 patients, with sequences as Fluid-Attenuated Inversion Recovery (FLAIR), T1-weighted, T1-weighted with contrast enhancement (T1ce), and T2-weighted. Of these, 484 cases are manually labeled. For model training and validation, 384 cases (80%) are allocated for training, and 100 cases (20%) for validation.

## 4.2 Data Preparation

As mentioned earlier, the **Picai-2022** dataset includes three modalities: T2w images, ADC, and HBV maps for each patient. To ensure uniformity, ADC and HBV maps are resampled using the maximum voxel spacing (43%) observed from axial T2W images, resulting in a voxel size of 3.0x0.5x0.5 mm. A two-step normalization procedure is applied, consisting of min-max normalization followed by z-score normalization. After normalization, all images, labels, and prostate whole gland masks are resized to 30 x 256 x 256. A bounding box is

computed around the prostate whole gland mask and extended by 30 pixels in each direction. The prostate region is then extracted from the T2W, ADC, and HBV maps corresponding to the same slice, reducing image and mask size for quicker experimentation. These extracted regions are resized to  $24 \times 160 \times 128$  for segmentation model training. Finally, the N4 bias field correction filter is applied to the dataset to reduce bias corruption.

The **BraTS 2018** dataset consists of 4 modalities (T1-weighted, T1ce, T2-weighted, and FLAIR ) for each patient. To ensure pixel dimension uniformity between these modalities, the 4 modalities are resampled to  $1.0 \times 1.0 \times 1.0$  mm/voxel. A two-step normalizing procedure is also implemented here, as Pca dataset. After intensity normalization, all image modalities and labels are resized to  $155 \times 224 \times 224$  along z, x and y directions.

### 4.3 Experiment Design & Implementation

We use the Stochastic Gradient Descent (SGD) optimizer [16] for all training methods. The optimizer has a base learning rate of 0.01, a momentum of 0.9, a weight decay of 0.0001, and we train for 300 epochs. The training is conducted with a batch size of 1. In order to address the problem of over-fitting, we employ data augmentation methods such as random affine transformations, flipping, Gaussian noise, and intensity scaling. The experiments are carried out utilizing PyTorch 2.3.1 on a high-performance computer configuration, comprising an Intel Xeon 2.40 GHz processor, an NVIDIA RTX 3060 GPU, and 32 GB of RAM.

### 4.4 Evaluation Metrics:

Evaluation metrics are crucial for assessing the performance of segmentation models. In this study, we utilized four primary metrics: mean IoU, DSC, Sensitivity, and Specificity which are described in [4]. IoU and Dice Coefficient quantify the overlap between the ground truth and predicted output. Sensitivity measures the proportion of True Positives, while Specificity measures the proportion of True Negatives. Together, these metrics provide a comprehensive evaluation of the model’s effectiveness.

## 5 Result and Discussion

In this section, we present experiments demonstrating the benefits of integrating a dynamic focusing parameter and adaptive imbalance weighting into the regular Focal Loss (FL) function. We provide quantitative comparisons between conventional FL and A-FL across various datasets. Additionally, we conduct comparative analyses of A-FL against FL using different baseline models and other loss functions. We also evaluate qualitative examples and perform ablation studies to assess the impact of our A-FL function.

### 5.1 Quantitative Results Evaluation

Tables 1 and 2 present a quantitative comparison between the regular FL and our proposed A-FL on the Pical 2022 [20] and BraTS 2018 [9] datasets.

**Table 1.** The proposed A-FL’s performance was evaluated against the regular FL function using a ResNet50-encoded U-Net model on the Pical 2022 Dataset [20].

Loss Function	Evaluation Metrics			
	<i>IoU</i> ↑	<i>DSC</i> ↑	<i>Sensitivity</i> ↑	<i>Specificity</i> ↑
Focal Loss	0.641	0.715	0.924	0.9484
Our A-FL	<b>0.696</b>	<b>0.769</b>	<b>0.941</b>	<b>0.9489</b>

On the Pical 2020 dataset, A-FL achieves a 5.5% increase in IoU, a 5.4% rise in DSC, and a 1.7% boost in Sensitivity, demonstrating improved handling of small and irregular tumors. Additionally, a slight increase in Specificity (0.05%) indicates balanced performance.

On the BraTS 2018 dataset, A-FL shows a 5.2% improvement in IoU and a 3.8% increase in DSC, reflecting better segmentation accuracy. Despite a minor decrease in Sensitivity (1.2%), the gain in Specificity (1.1%) suggests fewer false positives and a more robust architecture. Table 3 presents a comparison of the

**Table 2.** The proposed A-FL function’s performance was evaluated against the regular FL function using a ResNet50-encoded UNet model on the BraTS 2018 Dataset [9].

Loss Function	Evaluation Metrics			
	<i>IoU</i> ↑	<i>Dice</i> ↑	<i>Sensitivity</i> ↑	<i>Specificity</i> ↑
FL	0.831	0.893	<b>0.949</b>	0.946
A-FL	<b>0.883</b>	<b>0.931</b>	0.937	<b>0.957</b>

performance of the proposed Adaptive Focal Loss (A-FL) against several baseline loss functions, using a ResNet50-encoded U-Net model on the Pical 2022 dataset. The results show A-FL’s superiority in key metrics: IoU, Dice coefficient, and Sensitivity. Specifically, A-FL achieves an IoU of 0.696 and a Dice coefficient of 0.769, outperforming other loss functions such as Traversky Loss (IoU: 0.654, Dice: 0.726), Cross Entropy Loss (IoU: 0.630, Dice: 0.705), IoU Loss (IoU: 0.654, Dice: 0.727), Dice Loss (IoU: 0.665, Dice: 0.739), Dice Cross Entropy Loss (IoU: 0.670, Dice: 0.742), and Dice Focal Loss (IoU: 0.685, Dice: 0.757).

A-FL also achieves the highest Sensitivity at 0.951, indicating its accuracy in identifying true positives. Compared to the best-performing baseline, Dice Focal Loss, A-FL improves IoU by 1.61%, Dice coefficient by 1.58%, and Sensitivity by 6.14%. Although A-FL’s Specificity (0.948) is slightly lower than Dice Loss (0.952), it maintains high performance overall.

In Table 4, we compare A-FL with traditional Focal Loss (FL) using various baseline models on the Pica1 2022 dataset. The data highlights significant improvements in IoU, Dice coefficient, Sensitivity, and Specificity achieved by A-FL.

**Table 3.** Comparison studies evaluate the performance of the proposed A-FL against other baseline loss functions using a ResNet50-encoded U-Net model.

Loss Function	Evaluation Metrics			
	<i>IoU</i> $\uparrow$	<i>Dice</i> $\uparrow$	<i>Sensitivity</i> $\uparrow$	<i>Specificity</i> $\uparrow$
Traversky Loss	0.654	0.726	0.917	0.948
Cross Entropy Loss	0.630	0.705	0.870	0.876
IoU Loss	0.654	0.727	0.917	0.947
Dice Loss	0.665	0.739	0.904	<b>0.952</b>
Dice Cross Entropy Loss	0.670	0.742	0.938	0.927
Dice Focal Loss	0.685	0.757	0.896	0.949
A-FL	<b>0.696</b>	<b>0.769</b>	<b>0.951</b>	0.948

**Table 4.** Comparison studies for the performance of our proposed Loss function with the Focal Loss function using various baseline models.

Model	Loss Function	Evaluation Metrics			
		<i>IoU</i> $\uparrow$	<i>Dice</i> $\uparrow$	<i>Sensitivity</i> $\uparrow$	<i>Specificity</i> $\uparrow$
UNet	FL	0.640	0.710	0.721	0.749
	A-FL	<b>0.669</b>	<b>0.740</b>	<b>0.792</b>	<b>0.825</b>
AttUNet	FL	0.647	0.721	<b>0.997</b>	0.940
	A-FL	<b>0.679</b>	<b>0.750</b>	0.992	<b>0.948</b>
RegUNet	FL	0.562	0.622	0.600	<b>0.950</b>
	A-FL	<b>0.573</b>	<b>0.635</b>	<b>0.691</b>	0.944
RRUNet	FL	0.634	0.709	0.967	0.946
	A-FL	<b>0.672</b>	<b>0.740</b>	<b>0.989</b>	<b>0.949</b>
ResNet50 encoded UNet	FL	0.641	0.715	0.924	0.9484
	A-FL	<b>0.696</b>	<b>0.769</b>	<b>0.941</b>	<b>0.9489</b>

For the UNet model, A-FL improves IoU by 2.9% (from 0.640 to 0.669) and Dice coefficient by 3.0% (from 0.710 to 0.740). Sensitivity increases by 7.1% (from 0.721 to 0.792), and Specificity by 7.6% (from 0.749 to 0.825). For the AttUNet model, A-FL increases IoU by 3.2% (from 0.647 to 0.679) and Dice coefficient by 2.9% (from 0.721 to 0.750). Sensitivity slightly decreases by 0.5% (from 0.997 to 0.992), but Specificity improves by 0.85% (from 0.940 to 0.948). For the RegUNet model, A-FL improves IoU by 1.96% (from 0.562 to 0.573) and Dice coefficient by 1.3% (from 0.622 to 0.635). Sensitivity increases by 9.1% (from 0.600 to 0.691), while Specificity decreases by 0.63% (from 0.950 to 0.944). For the RRUNet model, A-FL enhances IoU by 3.8% (from 0.634 to 0.672) and

Dice coefficient by 3.1% (from 0.709 to 0.740). Sensitivity increases by 2.28% (from 0.967 to 0.989), and Specificity by 0.32% (from 0.946 to 0.949).

For the ResNet50 encoded UNet model, A-FL improves IoU by 5.51% (from 0.641 to 0.696) and Dice coefficient by 4.8% (from 0.715 to 0.769). Sensitivity increases by 1.84% (from 0.924 to 0.941), and Specificity slightly by 0.05% (from 0.9484 to 0.9489).

Tables 1, 2, 3, and 4 provide evidence for the superiority of A-FL in segmentation tasks, showing significant improvements in IoU, Dice coefficient, and Sensitivity across datasets, loss functions, and models. These results highlight A-FL’s effectiveness in handling class imbalance and enhancing performance in small volume and irregular tumor segmentation.

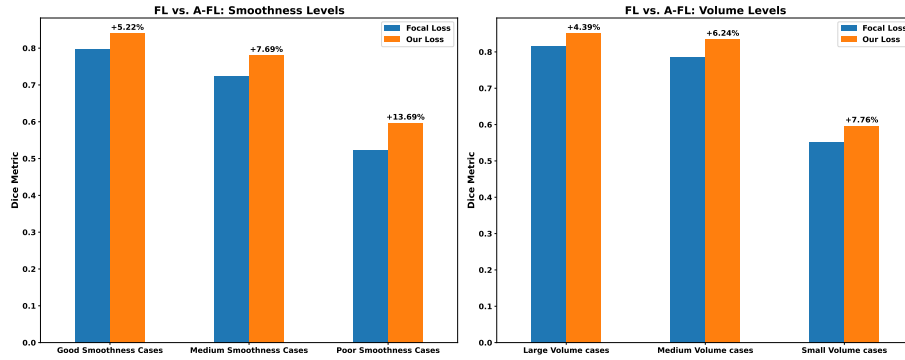


**Fig. 3.** Performance Comparison of Regular Focal Loss vs. Adaptive Focal Loss (A-FL). The left chart shows average Dice Similarity Coefficient (DSC) for good, medium, and poor smoothness cases. The right chart shows average DSC for large, medium, and small volume cases. Results highlight A-FL’s effectiveness in improving segmentation accuracy, especially for small volume and irregularly shaped tumors.

The bar charts in Fig. 3 compare traditional Focal Loss (FL) and our Adaptive Focal Loss (A-FL) using the Dice Similarity Coefficient (DSC) across different tumor smoothness and volume levels. For smoothness, A-FL demonstrates clear superiority, with a 5.22% improvement in DSC for tumors with good smoothness, a 7.69% improvement for medium smoothness tumors, and a notable 13.69% increase for tumors with poor smoothness. This highlights A-FL’s exceptional ability to manage tumors with varying surface complexities, particularly those with poor smoothness. In terms of volume, A-FL shows robust performance, providing a 4.41% improvement in DSC for large volume tumors, a 6.23% increase for medium volume tumors, and an impressive 7.77% boost for small volume tumors. These findings underscore A-FL’s effectiveness in accurately segmenting tumors of different sizes, excelling especially with smaller, more challenging tumors.

## 5.2 Qualitative Results Evaluation

The qualitative results for the Picai dataset, shown in Fig. 4, illustrate that A-FL outperforms baseline FL in prostate cancer (PCa) segmentation. While large volume and smooth surface cases (i) and (iii) show similar performance for both methods, A-FL excels in segmenting uneven or small volume tumors (cases (ii) and (iv)). This is evident in the 2D slice-by-slice visualizations, where A-FL demonstrates higher accuracy due to the dynamically adjusted focusing parameter.

In summary, the visual results in Fig. 4 support our quantitative findings, highlighting A-FL’s superior performance in managing various tumor volumes and surface complexities.

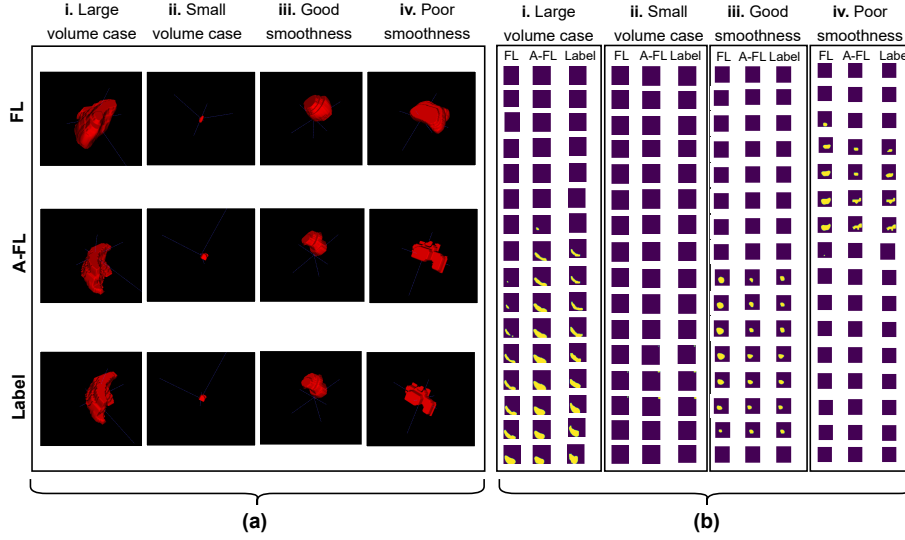


**Fig. 4.** (a) Qualitative results are visualized in 3D voxel and 2D slice manners for examples from the Picai validation set. In the 3D voxel visualization (a), the *Label* row shows ground truth masks, the *A-FL* row shows predictions using our proposed A-FL method, and the *FL* row shows predictions using the existing baseline FL. Columns represent large volume (i), small volume (ii), good surface smoothness (iii), and poor surface smoothness (iv) cases. In the 2D slice visualization (b), each bounded box-column follows the same order: baseline FL prediction, A-FL prediction, and ground truth mask.

## 5.3 The Ablation Studies

To assess the effectiveness of proposed dynamically tumor volume and smoothness adaptive focal loss (A-FL), twelve different experiments are conducted and

presented on Table-5. Each variable and combination of variables is tested with ResNet50 encoded U-Net architecture. The accuracy is measured by mean IoU and mean Dice from the respective dataset.

In Table 5, the first row is the baseline results using the original Focal Loss (FL) in where  $\alpha$  and  $\gamma$  is manually set to 0.25 and 2 respectively [7]. while the 2nd row shows the results after introducing  $\alpha_{va}$  alone which leads to a slight improvements due to assigning higher weights to minority foreground class. On the Pical dataset, IoU increased by 1.3% and Dice by 1.8%, while on the BraTS dataset, IoU increased by 0.7% and Dice by 1.3%.

Combining the background volume adapting weight  $\alpha_{va}$  with the foreground volume adapting weight  $\gamma_{va}$  improves results by balancing both background and foreground adjustments, leading to more precise segmentation. This increased IoU by 3.6% and Dice by 3.3% on the Pical dataset, and IoU by 1.5% and Dice by 1.9% on the BraTS dataset. Similarly, combining  $\alpha_{va}$  with the most influential parameter of our A-FL, tumor surface mean smoothness adapting weight  $\gamma_{mSa}$  enhances performance by ensuring more focus regarding more zigzag shaped tumor, increasing IoU by 4.6% and Dice by 4.1% on the Pical dataset, and IoU by 2.6% and Dice by 3.6% on the BraTS dataset.

The optimal configuration is achieved when all three parameters are enabled (shows in row 4), resulting in the highest metrics. Compared to the baseline, IoU on the Pical dataset increased by 5.5% and Dice by 5.4%, while on the BraTS dataset, IoU increased by 5.2% and Dice by 4.8%. Conversely, disabling  $\alpha_{va}$  while enabling both  $\gamma_{va}$  and  $\gamma_{mSa}$  results in lower performance compared to the optimal configuration. This demonstrates the effectiveness of dynamic parameter adjustments in addressing class imbalance and complex tumor structures.

**Table 5.** Ablation studies on Pical and BraTS dataset. Here, the values of  $\alpha_{va}$ ,  $\gamma_{va}$  and  $\gamma_{mSa}$  are continuously changed for every patient in the training session.

Parameters			Pical Dataset		BraTS Dataset	
$\alpha_{va}$	$\gamma_{va}$	$\gamma_{mSa}$	<i>IoU</i> ↑	<i>Dice</i> ↑	<i>IoU</i> ↑	<i>Dice</i> ↑
✗	✗	✗	0.641	0.715	0.831	0.883
✓	✗	✗	0.656	0.733	0.838	0.906
✓	✓	✗	0.677	0.748	0.846	0.912
✓	✗	✓	0.687	0.756	0.857	0.929
✓	✓	✓	<b>0.696</b>	<b>0.769</b>	<b>0.883</b>	<b>0.931</b>
✗	✓	✓	0.677	0.746	0.882	0.924

## 6 Conclusion

This paper introduces A-FL, a novel Adaptive Focal Loss (A-FL) function tailored for semantic segmentation, specifically addressing tumor volume and surface smoothness considerations. A-FL improves upon traditional focal loss by dynamically adjusting focusing and balancing parameters at the pixel level during

training. This adaptation allows our models to achieve more balanced and precise segmentation performance by integrating tumor volume and surface smoothness as focal parameters, while also considering background volume for class balancing. Experimental evaluations conducted on the PicaI and BraTS datasets using ResNet50-based U-Net architecture demonstrate the superior performance of A-FL compared to conventional focal loss methods.

## 7 Acknowledgments

This research is funded by Grant No. 56.00.0000.052.33.001.23-59 from the ICT Division, Bangladesh. The authors thank the Computer Vision & Intelligent Interfacing (CVIIL) Lab, Islamic University, Bangladesh for providing high-configuration computer setup for experiments. Special thanks to Biomedical Robotics, AI, and Imaging Network (BioRain) Lab and SAIVT, QUT for their ongoing support, contributions to the study design, and project supervision.

## References

1. Hassan, R., Mondal, M.R.H., Ahamed, S.I.: Udbnet: A novel uncertainty driven boundary refined network for organ at risk segmentation. PLOS ONE **19**(6), 1–18 (06 2024). <https://doi.org/10.1371/journal.pone.0304771>
2. He, K., Zhang, X., Ren, S., Sun, J.: Deep residual learning for image recognition. In: Proceedings of the IEEE conference on computer vision and pattern recognition. pp. 770–778 (2016)
3. Ho, Y., Wooley, S.: The real-world-weight cross-entropy loss function: Modeling the costs of mislabeling. IEEE access **8**, 4806–4813 (2019)
4. Jadon, S.: A survey of loss functions for semantic segmentation. In: 2020 IEEE conference on computational intelligence in bioinformatics and computational biology (CIBCB). pp. 1–7. IEEE (2020)
5. Leng, Z., Tan, M., Liu, C., Cubuk, E.D., Shi, X., Cheng, S., Anguelov, D.: Polyloss: A polynomial expansion perspective of classification loss functions. arXiv preprint arXiv:2204.12511 (2022)
6. Lin, J., Xiao, Z., Wei, X., Duan, P., He, X., Dian, R., Li, Z., Li, S.: Click-pixel cognition fusion network with balanced cut for interactive image segmentation. IEEE Transactions on Image Processing **33**, 177–190 (2023)
7. Lin, T.Y., Goyal, P., Girshick, R., He, K., Dollár, P.: Focal loss for dense object detection. In: Proceedings of the IEEE international conference on computer vision. pp. 2980–2988 (2017)
8. Maninis, K.K., Caelles, S., Pont-Tuset, J., Van Gool, L.: Deep extreme cut: From extreme points to object segmentation. In: Proceedings of the IEEE conference on computer vision and pattern recognition. pp. 616–625 (2018)
9. Menze, B.H., Jakab, A., Bauer, S., Kalpathy-Cramer, J., Farahani, K., Kirby, J., Burren, Y., Porz, N., Slotboom, J., Wiest, R., et al.: The multimodal brain tumor image segmentation benchmark (brats). IEEE transactions on medical imaging **34**(10), 1993–2024 (2014)
10. Milletari, F., Navab, N., Ahmadi, S.A.: V-net: Fully convolutional neural networks for volumetric medical image segmentation. In: 2016 fourth international conference on 3D vision (3DV). pp. 565–571. Ieee (2016)

11. Minaee, S., Boykov, Y., Porikli, F., Plaza, A., Kehtarnavaz, N., Terzopoulos, D.: Image segmentation using deep learning: A survey. *IEEE transactions on pattern analysis and machine intelligence* **44**(7), 3523–3542 (2021)
12. Nazib, A., Hassan, R., Islam, Z., Fookes, C.: Uncertainty driven bottleneck attention u-net for organ at risk segmentation (2024)
13. Pais, G.D., Ramalingam, S., Govindu, V.M., Nascimento, J.C., Chellappa, R., Miraldo, P.: 3dregnet: A deep neural network for 3d point registration. In: *Proceedings of the IEEE/CVF conference on computer vision and pattern recognition*. pp. 7193–7203 (2020)
14. Pihur, V., Datta, S., Datta, S.: Weighted rank aggregation of cluster validation measures: a monte carlo cross-entropy approach. *Bioinformatics* **23**(13), 1607–1615 (2007)
15. Rahman, M.A., Wang, Y.: Optimizing intersection-over-union in deep neural networks for image segmentation. In: *International symposium on visual computing*. pp. 234–244. Springer (2016)
16. Robbins, H., Monro, S.: A stochastic approximation method. *The annals of mathematical statistics* pp. 400–407 (1951)
17. Ronneberger, O., Fischer, P., Brox, T.: U-net: Convolutional networks for biomedical image segmentation. In: *Medical image computing and computer-assisted intervention—MICCAI 2015: 18th international conference, Munich, Germany, October 5–9, 2015, proceedings, part III* 18. pp. 234–241. Springer (2015)
18. Roy, R., Annappa, B., Dodia, S.: 3d attu-net for brain tumor segmentation with a novel loss function. In: *2023 6th International Conference on Information Systems and Computer Networks (ISCON)*. pp. 1–8. IEEE (2023)
19. Ruby, U., Yendapalli, V.: Binary cross entropy with deep learning technique for image classification. *Int. J. Adv. Trends Comput. Sci. Eng* **9**(10) (2020)
20. Saha, A., Bosma, J.S., Twilt, J.J., van Ginneken, B., the PI-CAI consortium: Artificial intelligence and radiologists in prostate cancer detection on mri (pi-cai): an international, paired, non-inferiority, confirmatory study. *The Lancet Oncology* **25**(7), 879–887 (2024). [https://doi.org/https://doi.org/10.1016/S1470-2045\(24\)00220-1](https://doi.org/https://doi.org/10.1016/S1470-2045(24)00220-1)
21. Santambrogio, F.: {Euclidean, metric, and Wasserstein} gradient flows: an overview. *Bulletin of Mathematical Sciences* **7**, 87–154 (2017)
22. Sofiiuk, K., Barinova, O., Konushin, A.: Adaptis: Adaptive instance selection network. In: *Proceedings of the IEEE/CVF international conference on computer vision*. pp. 7355–7363 (2019)
23. Sudre, C.H., Li, W., Vercauteren, T., Ourselin, S., Jorge Cardoso, M.: Generalised dice overlap as a deep learning loss function for highly unbalanced segmentations. In: *Deep Learning in Medical Image Analysis and Multimodal Learning for Clinical Decision Support: Third International Workshop, DLMIA 2017, and 7th International Workshop, ML-CDS 2017, Held in Conjunction with MICCAI 2017, Québec City, QC, Canada, September 14, Proceedings 3*. pp. 240–248. Springer (2017)
24. Wu, D., Zhang, R., Pore, A., Dall’Alba, D., Ha, X.T., Li, Z., Zhang, Y., Herrera, F., Ourak, M., Kowalczyk, W., et al.: A review on machine learning in flexible surgical and interventional robots: Where we are and where we are going. *Biomedical Signal Processing and Control* **93**, 106179 (2024)
25. Xie, S., Tu, Z.: Holistically-nested edge detection. In: *Proceedings of the IEEE international conference on computer vision*. pp. 1395–1403 (2015)
26. Zhang, Y., Shen, Z., Jiao, R.: Segment anything model for medical image segmentation: Current applications and future directions. *Computers in Biology and Medicine* p. 108238 (2024)